IEEE Open Journal of the
Solid-State Circuits Society

Received 12 May 2023; revised 9 August 2023; accepted 6 September 2023. Date of publication 11 September 2023; date of current version 31 October 2023.

*Digital Object Identifier 10.1109/OJSSCS.2023.3313575*

# Recent Trends and Challenges in Near-Field Wireless Power Transfer Systems

**ELISABETTA MOISELLO (Member, IEEE), ALESSANDRO LIOTTA (Graduate Student Member, IEEE), PIERO MALCOVATI (Senior Member, IEEE), AND EDOARDO BONIZZONI (Senior Member, IEEE)**

*(Invited Paper)*

Department of Electrical, Computer and Biomedical Engineering, University of Pavia, 27100 Pavia, Italy

CORRESPONDING AUTHOR: E. MOISELLO (e-mail: elisabetta.moisello@unipv.it)

**ABSTRACT** In recent years, wireless power transfer (WPT) has become a widespread method for charging and powering devices, including but not limited to consumer electronics, industrial applications, electric vehicles, medical devices, and sensor nodes. This article provides an overview of the available WPT technologies, focusing on the near-field case, and highlights the main architecture and circuit-level challenges encountered in the implementation of magnetic-based near-field WPT systems while reviewing the proposed solutions in the literature, in order to identify the main research interests as well as the trends for the future.

**INDEX TERMS** Coil, inductive, near-field, rectifier, regulation, resonant, wireless charging, wireless data transfer, wireless power transfer (WPT).

## I. INTRODUCTION

WIRELESS power transfer (WPT) enables the charging and powering of devices while avoiding cables and bulky connections, thus improving user-friendliness. Furthermore, the device size can be reduced as the battery module can be scaled down, relying on the fact that the device lifetime is no longer dependent on the battery life itself. Hence, WPT has gained considerable relevance in recent years and has become a focus in both research and commercial product development, as cables can be inconvenient and unreliable over time, due to wear and tear, and increasingly smaller devices are preferred. With respect to cable-based solutions, WPT instead ensures high durability and reliability, in particular in hostile environments, such as the case for undersea applications [1]. Indeed, the device can be completely sealed and, therefore, protected from outside agents, such as dust or humidity, as it happens in the case of wireless solid-state drive (SSD) devices [2]. Moreover, along with WPT, also wireless communication between the power transmitter and receiver (and vice versa) can be supported: hence, power can be provided to the receiver in an on-demand fashion depending on its needs, as they can be conveyed to the transmitter by wireless communication. In this way, the device charging can also be more flexible and energy efficient.

WPT has become widespread in consumer electronics (i.e., smartphones and smartwatches) [3], while wireless charging for electric vehicles (EVs) is emerging as a hot topic, in view of the desire to abandon conventional internal combustion engine vehicles in favor of EV, with the final goal of implementing roadway-powered electric vehicles in order to be able to downsize the battery and avoid waiting time for charging when needed [4]. WPT is also well suited for powering sensor nodes in order to provide reliable long-term health and environmental monitoring [5], [6]. Furthermore, WPT enables the employment of medical implantable devices without the need to replace them when the battery's power has been depleted [7], [8], thus reducing the discomfort and health risk posed to the patient. Indeed deep brain stimulation devices are becoming popular for relieving and inhibiting the aggravation of some diseases (e.g., Parkinson's disease, tremor, dystonia, and chronic pain), but a surgical procedure is required for the device implantation, which puts the patient under significant health risks every time the device has to be replaced: WPT would enable single device implantation as the device battery could be then recharged when required, without needing to replace the implanted device.

A typical WPT system is schematically illustrated in Fig. 1. The input voltage generator $V_{in}$ provides the power

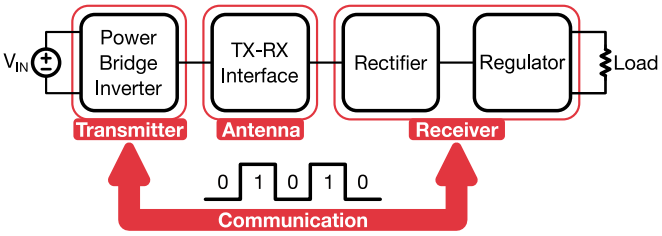


FIGURE 1. Block diagram of a typical WPT system.

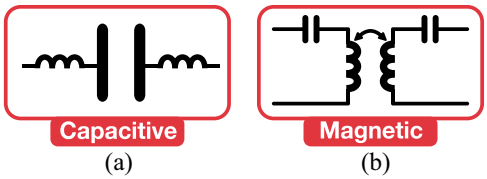


FIGURE 2. Schematic representation of the antenna block with series compensation circuit for the (a) capacitive and (b) magnetic coupling case.

to be transferred by the transmitter (TX) to the receiver (RX) through the antenna block, which realizes the interface between TX and RX while also implementing compensation and impedance matching. The TX usually consists of a power bridge inverter, while the RX includes a rectifier and a regulator, in order to provide the desired voltage at the load. A bidirectional communication channel between TX and RX, if present, allows for adjusting the transmitted power depending on the RX demands and TX capabilities.

In recent years, the research interest has focused on optimizing the blocks required for implementing WPT systems, in particular on the RX and the antenna, while investigating the best approach for providing the WPT. This article aims at highlighting the main challenges encountered in the design of a subset of WPT systems, the ones based on near-field operation, while reviewing the solutions proposed in the literature, in order to paint the picture of the current and future trends in the field. This article is organized as follows. Section II will provide an overview of the different WPT technologies and illustrate in detail the near-field approaches for providing the coupling between TX and RX, resulting in different standards, highlighting their advantages and drawbacks, while Section III will analyze the main critical challenges in near-field WPT systems design, reviewing the various solutions proposed in the literature to tackle the issues. Section IV will provide an overview of the state-of-the-art, illustrating the current trends, and Section V will conclude this article.

## II. WIRELESS POWER TRANSFER TECHNOLOGIES

WPT can be mainly classified into radiative, or radio-frequency (RF)-based, techniques and nonradiative approaches, consisting of inductive coupling, magnetic resonance coupling, and capacitive coupling [9].

Radiative WPT relies on the electric field of electromagnetic waves, typically RF waves or microwaves in the 300-MHz–300-GHz frequency range, as the medium for delivering energy. Radiative techniques support omnidirectional or directive, beamforming-based [10], power radiation: both approaches work in the far-field region, over large distances, where the power decreases according to the square of the reciprocal of the TX–RX distance and the absorption of radiation does not affect the TX, as TX and RX are not coupled. Because of the safety issues and health risks determined by RF exposure [11], radiative WPT is mainly limited to low power levels applications, e.g., sensor nodes with up to 10-mW power consumption [9].

When high power levels are targeted, nonradiative WPT is generally required: as it works in the near-field region, where the power is attenuated according to the cube of the reciprocal of the TX–RX distance, relatively small distances between TX and RX are supported. Since in nonradiative WPT the TX and RX are coupled, the radiation absorption in the RX affects the TX as well. Capacitive coupling relies on the electric field, while inductive and magnetic resonance coupling, as the names suggest, exploits the magnetic field.

Capacitive WPT is not widely employed as, in order to achieve a good coupling, relatively large coupling areas are required unless an operating frequency in the MHz range is selected: this type of WPT technology, therefore, is not suitable for typical-size portable electronic devices, as it would result in insufficient power density values [3], [9]; it has been employed, instead, for on-orbit applications [12], for low-power solutions, such as USB devices, lamps, and small robots [13] and for selected biomedical applications, such as multichannel nerve/muscle stimulation or those with multiple light-emitting diodes for optogenetics [14]. The advantage of capacitive WPT lies in the avoidance of the undesired eddy currents and electromagnetic interferences (EMIs) that come with magnetic-based WPT methods: in this way, capacitive charging can allow energy transfer also through metal [3], [15]. Capacitive power transfer antenna blocks are made up of two aligned conductive parallel plates, featuring the same surface area, separated by a gap, usually in the order of the millimeter range [13], [16]. In addition to the coupling capacitor, a compensation circuit is added to provide resonant conditions for the capacitor [13]: a schematic representation of the capacitive power transfer antenna including the most widely used compensation circuit topology, i.e., an inductor connected in series with the coupling capacitor to achieve a series resonance, is reported in Fig. 2(a).

Magnetic coupling-based systems, relying on the coupling of the magnetic field between two coils, are the most widespread implementation of WPT applications [9]. The antenna block in inductive and magnetic resonance-based WPT systems consists of two coupling coils and a compensation circuit made up of capacitors: conventionally, a single capacitor is connected in series (S) or parallel (P) with the coil, giving rise to four topologies (S-S, S-P, P-S, and P-P) depending on the employed connections for the TX and

RX coils, respectively; however, a topology including more than one capacitor can also be employed (e.g., S-SP) [13]. The S-S topology, which is the most common, is illustrated schematically in Fig. 2(b). Although the same antenna structure is employed for both inductive and magnetic resonant WPT technologies, the two methods differ significantly as a result of the chosen frequency of operation with respect to the resonant frequency of the antenna: indeed in magnetic resonant systems, the operating frequency and the antenna frequency coincide, while inductive systems operate at frequencies away from the antenna resonance frequency.

Inductive WPT occurs when the TX coil generates a varying magnetic field across the RX coil within the field, thus inducing a voltage/current, thanks to the near-field magnetic power. The operating frequencies for inductive WPT are in the kHz range. High power transfer and high efficiency, exceeding 90%, are achieved, provided that the coils are strongly coupled (the typically achieved coupling coefficient $k$ is 0.7 in this case): for achieving such coupling the coils need to be aligned and in close proximity to each other, thus also ensuring safety for surrounding people. The Qi standard [3], launched by the Wireless Power Consortium in 2010, acts as a reference for inductive WPT for consumer electronics: for conventional Qi applications, the operating frequency is 100–300 kHz, with a resonant RX antenna frequency typically lower (e.g., for a 140-kHz operating frequency the RX antenna resonance frequency is roughly 80 kHz). In order to ensure the required high coupling coefficient, sockets for accommodating the load or magnets to guide the RX in the desired position, ensuring optimal alignment and TX–RX distance, are used.

In order to support the free positioning of the RX with respect to the TX, considering both distance and possible misalignment, resonant magnetic coupling was introduced. Magnetic resonance is based on evanescent wave coupling, which generates and transfers electrical energy between two resonant coils through varying or oscillating magnetic fields [9]. Magnetic-resonance-based WPT systems allow transferring power over larger distances with respect to the case of the inductive method, while also requiring less precise alignment [17]: indeed high-quality factor resonators are chosen, as it helps to compensate for the decrease in coupling coefficient [9]. In order to achieve high-quality factors, operating, and thus resonant, frequencies in the MHz range are required. Thanks to the properties of resonance, magnetic resonance coupling allows achieving better immunity from neighboring environmental disturbances; furthermore, since magnetic resonance coupling can be supported between one TX resonator and multiple RX resonators, magnetic resonance WPT systems can enable the concurrent charging of multiple devices [9]. The cost of obtaining improved spatial freedom is a decrease in efficiency with respect to the inductive case with strongly coupled coils [17]. The reference standard for resonant WPT is the one developed by the AirFuel Alliance [18], which supposes a 6.78-MHz (and its multiples) operating frequency.

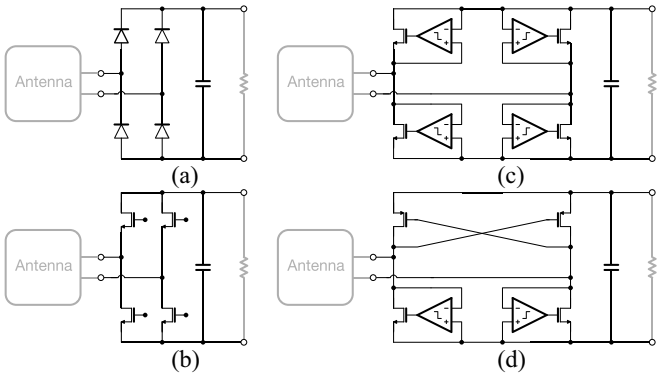


**FIGURE 3.** Schematic representations of (a) diode full-bridge rectifier, (b) active rectifier, (c) active rectifier with a dedicated comparator for each switch, and (d) cross-connected active rectifier.

In addition to the mentioned techniques, WPT technologies, such as ultrasound-based [19], [20], [21] and laser-based approaches [22], [23], are also emerging: these new approaches, however, are still in the early stages of development and have not yet been commercialized.

As inductive and resonant systems are the most common implementations for WPT, the Qi and the Airfuel standards constitute the reference for commercial WPT solutions, especially for what concerns consumer electronics. Given that the market and research focus is mainly oriented to near-field and in particular magnetic coupling-based solutions, the remainder of this article will consider magnetic-coupling-based systems, unless stated otherwise.

## III. CHALLENGES IN NEAR-FIELD WIRELESS POWER TRANSFER SYSTEMS

Different challenges are encountered in the design and implementation of near-field WPT systems: in particular, the rectifier circuit block, the RX-side and TX-side regulation, required to overcome misalignment issues, the data transmission over the TX–RX communication channel and the support of multiple standards, multiple loads, and multiple directions in WPT can be identified. These challenges and the proposed solutions in the literature are now reviewed in detail.

### A. RECTIFIER CIRCUIT

The baseline solution for implementing the rectifier is employing four diodes in a bridge configuration, as illustrated in Fig. 3(a), with a sufficiently large capacitor connected at the output to provide filtering. This implementation, however, suffers a significant drawback, that is the efficiency loss determined by the voltage drop on the diodes. In order to solve this issue, the diodes can be replaced by appropriately controlled MOS transistors acting as power switches, as shown schematically in Fig. 3(b), where nMOS devices are employed for all switches, as they typically feature a better figure of merit; alternatively, pMOS devices can be used for implementing the high-side switches, while nMOS

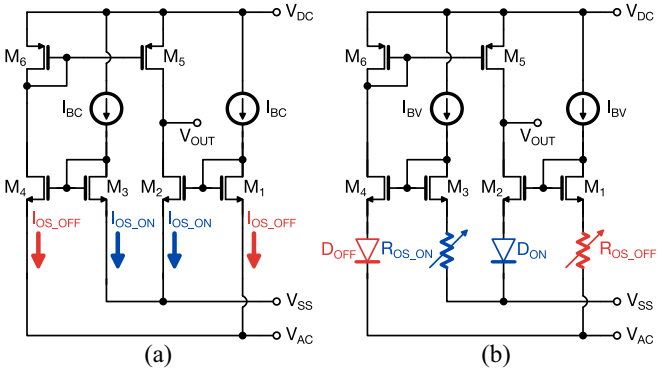


**FIGURE 4.** Schematic representations of (a) CM and (b) VM delay compensation implementation, where $V_{OUT}$ is the comparator output and $V_{AC}$ and $V_{SS}$ are the comparator inputs. $V_{SS}$ is the switch source node and $V_{AC}$ is the switch drain node, connected to the antenna.

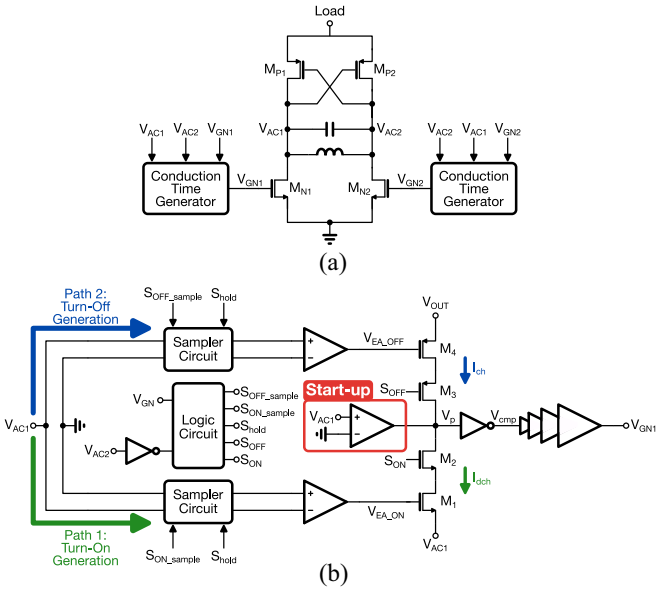


**FIGURE 5.** Schematic representations of the (a) active rectifier and (b) inverter-based conduction-time generator proposed in [24] for implementing the active rectifier control.

are employed for the low-side ones. In order to achieve high efficiency, it is desired to control the switches so that they act as equivalent "active" diodes (i.e., they need to be on when conducting a positive current from the source to the drain), ensuring zero-voltage switching (ZVS) operation for the switches: for this reason, this rectifier solution is referred to as active rectifier. For controlling the switches, a comparator for each switch can be employed [25], as shown in Fig. 3(c), or two comparators can be used in order to command the low-side or high-side switches, while the high-side or low-side transistors, respectively, form a cross-connected structure [14], [26], [27], [28], [29], [30], as illustrated in the example reported in Fig. 3(d). Cross-connected structures feature the advantage of self-driving of the cross-connected switch pair, however, their employment is limited to cases where the desired output voltage is low and does not exceed the maximum supported gate-to-source voltage of the used transistors: this case is quite common in the literature, since it is typically satisfied for biomedical and implantable devices, that have been a hot topic in recent years given the increasing interest on brain–machine interfaces [26].

Independently from the number of comparators used, it is necessary to compensate for the active diode delay in turning on/off, which would give rise to multiple pulsing and reverse current issues, that would severely impact the circuit efficiency [26]. There exist two main techniques in order to compensate for the on/off-delay: 1) current mode (CM) and 2) voltage mode (VM) compensation [30], which are illustrated schematically in Fig. 4. CM delay compensation injects offset current to generate offset voltage at the input of the comparator at the rising/falling edges of the active diode control signal, thus causing an earlier comparator commutation; VM compensation works in a similar way: instead of using offset currents, it directly introduces offset voltage by means of resistors. CM compensation features advantages in terms of high compensation accuracy and wide compensation range (i.e., the rectifier can achieve high efficiency and voltage conversion ratio under a wide input power and load range); however, it requires larger power consumption with respect to VM, which, in turn, suffers from limited implementable offset range and accuracy. In order to find a tradeoff between power consumption and compensation range, CM and VM compensation techniques can be combined, e.g., using CM for on-delay and VM for off-delay compensation, as proposed in [30]. In order to minimize power consumption while using the CM approach, a switched-offset scheme was proposed in [26], where push–pull structures were employed for the differential common-gate comparators, as well as for the required dynamic switched current source determining the time-varying offset voltages at the comparator input. In order to be able to accurately compensate for both the on and off delays, also in the presence of PVT variations and mismatches, usually two feedback loops are implemented in order to generate the required on and off delays adaptively [14], [31], possibly regulating the delay digitally, as it was proposed in [29], where a SAR-assisted coarse–fine tuning is employed. In addition to the traditional CM and VM techniques, another approach relying on the use of controlled digital delay lines [32] and delay-locked loop (DLL) [33] was also proposed: this allows drastically reducing the power consumption as the power-hungry comparators are eliminated from the circuit. Other solutions for decreasing the power consumption include the use of dynamic common-gate comparators, thus avoiding static power consumption [27] and the adoption of an inverter-based conduction-time generator. The rectifier relying on the inverter-based conduction-time generator is shown schematically in Fig. 5: it consists of a current starving inverter cell, sample/hold loops, transconductance amplifiers, and a logic block, thus avoiding comparators and complicated logic modules [24].

In order to increase the circuit efficiency, switching losses can be reduced by employing negative impedance circuits [33] or the gate charge recycling technique, where switching losses are stored on a capacitor in one phase and then added to the rectified voltage in the other [34], [35].

Alternative rectifier implementations rely on a reconfigurable diode topology, which features both very low-threshold voltage and high tunable breakdown voltage [36]. The latter solution, however, cannot be adopted freely as the proposed topology consists of two Schottky diodes and two depletion-mode nMOS transistors, featuring a negative turn-on voltage, which are not available in all processes.

### B. RX-SIDE AND TX-SIDE REGULATION

In order to maintain the desired voltage at the RX output and provide over-voltage protection, local RX-side regulation is typically required in WPT systems. Usually, a separate block, cascaded after the rectifier circuit, is employed. The cascaded block can be either a low-dropout (LDO) regulator or a dc–dc converter [17], [33], [35], [37], [38], [39], [40], [41]: the LDO is simpler and more compact, at the cost of higher losses, while the dc–dc converter features better efficiency, but requires an extra inductor. dc–dc converters can implement buck [35], boost [41], or buck-boost [37] regulation.

Employing a multiple-stage structure in the RX, however, significantly lowers the efficiency, since the total efficiency is determined by the product of the efficiency of each stage. For this reason, research has focused on developing solutions where the rectification and RX-side regulation are implemented in a single circuit. A novel architecture merging an $N$-level single-inductor multiple-output (SIMO) dc–dc converter and a multistage rectifier was proposed in [42], where the prototype of an active voltage doubler rectifier, merged with a 3-level single-inductor dual-output (SIDO) converter, was presented. In general, regulating rectifiers typically allow controlling, by means of various techniques, the rectified current. A control approach is based on pulse width modulation (PWM), which controls the duty cycle of the rectifier switches, implementing different rectifier configurations and thus adjusting the impedance seen by the antenna, as shown in Fig. 6. Indeed, the main possible rectifier configurations illustrated in Fig. 6 are 1×, 0.5×, and 0×, which correspond, respectively, to a full-bridge rectifier, a half-bridge rectifier, and an antenna short circuit. An additional 2× configuration, corresponding to a voltage doubler made up of two half-bridge rectifiers connected in series, can also be implemented [43]. By switching between configurations, it is possible to regulate the average rectified load current and, therefore, the output voltage: Li et al. [43] employed 1×–2× configurations, [25] 0×–0.5×–1× configurations, and Yang et al. [44] and Namgoong et al. [45] employed 0×–1× configurations. In order to obtain the desired equivalent impedance adjustment, resulting in the output voltage control, phase shifting [39], [46], delay-tuning [47], constant-idle time

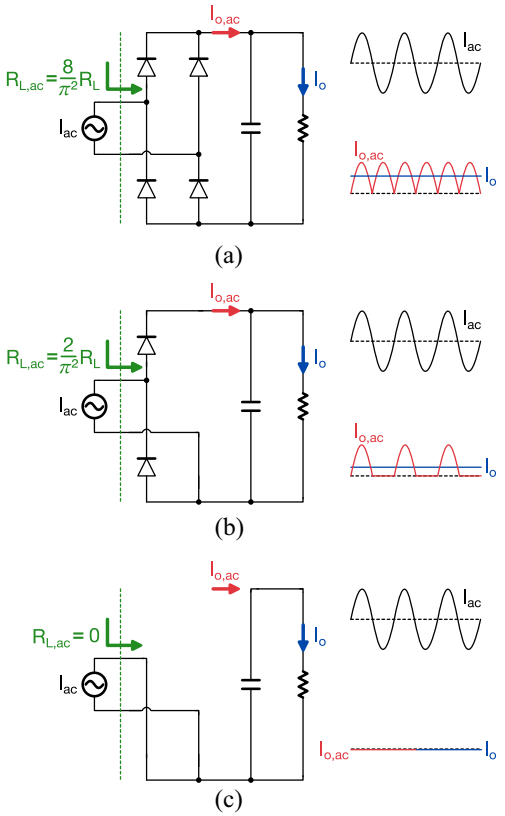


**FIGURE 6.** Regulating rectifier relying on PWM technique: (a) 1×, (b) 0.5×, and (c) 0× configurations.

control [40], [45], intentional reverse current [48], pulse-frequency modulation (PFM) [49], [50], and pulse skipping techniques [51] can also be employed. For achieving fast transient response a hysteretic control is preferred [45], [52].

Another regulation approach, available for magnetic resonance WPT systems, directly eliminates the rectifier circuit by rectifying the RX coil current, rather than the voltage [53]. This is achieved by a two-phase operation: during the first phase, energy is accumulated by resonating the LC tank for multiple cycles, while during the second phase, the energy is delivered to the load in a boost fashion when the resonant current is at its peak [54], [55], [56], as schematically illustrated in Fig. 7. However, with this solution, it is difficult to operate at high resonant frequencies because the detection of the resonant current peak becomes challenging due to the intrinsic delay and offset of the comparator used in the peak timing detector; moreover, an LC-tank resonance-loss interval is present, which negatively affects optimal power transfer from the TX to the RX since the reactive impedance is not canceled out but appears on the TX side; furthermore, during the LC-tank resonance-loss interval, the LC tank and the output are not isolated and, therefore, the power-transfer efficiency can be affected by load variations [57].

The considered regulation systems provide only a regulated voltage at the RX output, however battery charging, e.g., for lithium-ion batteries, typically requires adhering to a


**FIGURE 7.** Regulating rectifier relying on multicycle LC tank resonance.

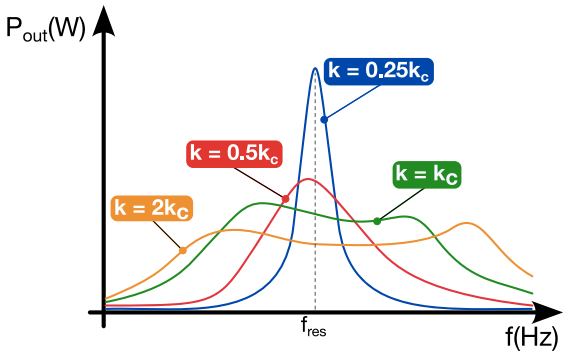


**FIGURE 8.** Schematic illustration of the frequency splitting phenomenon.

specific charging profile, which involves an initial constant-current (CC) charging phase and, when the battery is almost fully charged, a constant-voltage (CV) charging phase [58]. In order to implement the desired charging profile, an additional block is required at the load. However, an extra stage determines a decrease in efficiency. Hence, a solution implementing rectification, regulation, and CC/CV charging in a single stage was presented in [59]: a CC loop was added to the regulating rectifier structure, switching between $0\times$–$0.5\times$–$1\times$ modes, proposed in [25], thus enabling both CV and CC charging.

The local RX-side regulation, however, is not sufficient in most WPT systems: indeed, due to horizontal misalignments and varying distances between RX and TX, the coupling coefficient in near-field-based solutions can vary greatly, determining a load variation that affects the efficiency and delivered power level [60]. Local RX-side regulation is not able to support effectively the possible wide load variation range, hence, a TX-side regulation is also required: depending on information fed back by the RX to the TX, the TX-side control acts on the transmitted power in order to bring back the WPT to an optimum efficiency and/or power case, thus implementing efficiency and/or power tracking. The TX-side control can be implemented through a reconfigurable class-D power amplifier [45], [47], can act on the TX voltage by means of an additional converter circuit [61] or through phase shifting [62], or can regulate the operating frequency in order to track the frequency for which the maximum power can be transferred at the output load. Indeed, in resonant WPT systems, due to the frequency splitting phenomenon [63], the frequency corresponding to the maximum power transfer varies: as illustrated in Fig. 8, for coupling coefficients larger than a critical value $k_c$, the output load power curve as a function of operating frequency changes from a single-peak curve, with the peak corresponding to the nominal resonance frequency, to a double-peak curve, where the two peaks are at frequencies different from the resonant ones. By adjusting the operating frequency while maintaining a fixed coupling coefficient is therefore possible to vary the load power; moreover, when the coupling coefficient varies, it is also possible to track the frequency at which the maximum power can be delivered [64].

### C. TX–RX COMMUNICATION

In recent years, simultaneous wireless information and power transfer (SWIPT) systems have become increasingly important due to their ability to eliminate the need for wires and cables, making it easier to charge and communicate with devices. This can be especially important in applications, such as healthcare or industrial automation, where wires can be inconvenient or even dangerous.

As explained previously, SWIPT is fundamental for enabling effective RX-side regulation. Moreover, data transmission enriches the system capabilities providing additional monitoring and functionalities. For instance, in healthcare [43], [56], [65], [66], [67], [68], [69], [70], implantable medical devices, such as pacemakers, hearing aids, and neurostimulators can be wirelessly powered and communicate, enabling real-time monitoring and adjustment of treatment. Similarly, in transportation [71], [72], [73], [74], SWIPT systems can wirelessly charge electric vehicles and simultaneously transmit information, including vehicle performance data, charging history, and location. Finally, SWIPT technology is also employed in consumer electronics [75], [76], such as smartphones, smartwatches, and laptops, to wirelessly charge the devices while transmitting data, such as notifications and updates.

Although the Airfuel standard employs Bluetooth for data transfer, recent research in the field of SWIPT has focused on the development of WPT systems that can transfer data without relying on existing communication standards (i.e., Bluetooth, WiFi or RF links), as they can suffer from limitations in terms of pairings, bandwidth, range, and interference susceptibility.

SWIPT techniques can be classified into two main categories based on the number of channels used for power and data transfer. Single-channel power and data transfer involves using a single wireless channel for both power and data transfer. The main advantage of this approach is its simplicity, as it only requires a single channel for both power and data transfer, reducing the complexity of the system and lowering its cost. However, this method is only suitable for relatively low-power transmission, such as for consumer electronics, as the power voltage can create noise in the signal transmission, resulting in an excessively low signal-to-noise ratio (SNR) of the system. In contrast, the multiple channels category uses independent wireless channels for power and data transfer, providing a higher data rate and greater range than power carrier-based SWIPT. It can wirelessly transfer large amounts of power over longer distances

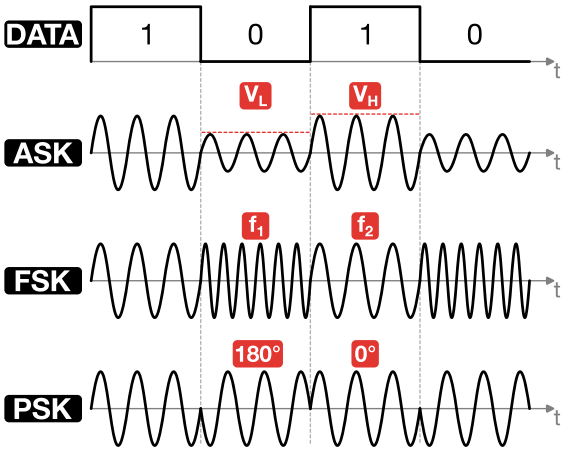


**FIGURE 9.** Most common power-carrier-based modulation methods employed in SWIPT systems.

while avoiding interference between power and data channels. As a result, it is better suited for high-power devices, such as electric vehicles or industrial automation systems.

Single-channel SWIPT techniques can be further classified into power carrier-based (PC-SWIPT) and high-frequency data-carrier-based SWIPT (HFDC-SWIPT) systems. The power carrier-based method involves modulating the power signal directly to generate the data signal, using the same carrier signal. This method is the one employed, for example, in the Qi standard. While this technique avoids interference issues between power and data signals, it has limited data transfer rates due to the bandwidth of the power carrier signal. Several modulation methods, depicted in Fig. 9, are available for SWIPT systems, such as amplitude-shift keying (ASK), frequency-shift keying (FSK) and phase-shift keying (PSK). Among these techniques, FSK [67], [68], [73], [75], [77], [78] has lower error susceptibility than ASK [69], [79] and simpler signal detection and recovery process than PSK [78], [80]. However, modulating the power carrier with a frequency other than the resonance frequency reduces efficiency. The binary FSK approach is used in [77], taking advantage of the dual band of a series–parallel combined resonant circuit to ensure efficiency. An envelope detector-based receiver and impedance matching controller for high efficiency, even with ASK modulation, are presented in [79]. In order to ensure optimal resonance and phase continuity in the inductor current at all times, both FSK and PSK modulations are utilized in [78]. The power carrier-based method is commonly used for downlink (TX to RX) communication. Indeed, the power transmitter modulates the power carrier and transmits it from TX to RX, enabling the transfer of data information while also delivering power to the load at the same time. Alternatively, for uplink (RX to TX) communication, the load-shift keying (LSK) modulation technique can be utilized. LSK is a variation of ASK modulation where the load on the receiver side is varied based on the data being transmitted to the primary side [43], [66], [70], [75].

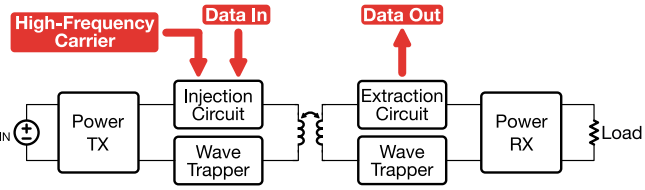


**FIGURE 10.** Block diagram of the downlink (TX to RX) high-frequency data-carrier-based SWIPT system.

High-frequency data-carrier-based SWIPT, illustrated schematically in Fig. 10, involves injecting a low-frequency data signal onto a high-frequency carrier signal using modulation techniques, which is then wirelessly transmitted between coils of a transformer and demodulated. This approach enables bidirectional communication (uplink and downlink) by inverting injection and extraction circuits. Additionally, independent control of power and data ensures both high power efficiency and data rate. However, interference between the power and data carriers can cause crosstalk and degrade the quality of the transmitted information. To avoid this issue, various techniques have been proposed. In [81], band-pass filters called wave trappers are added to filter out unwanted frequencies, while Wei et al. [82] utilized the double-D coupling coil's characteristic to directly inject data into one of the D coils without wave trappers. In [83], a power/data frequency division multiplexing technique is employed, where power and data are transmitted using different frequency carriers, allowing for independent control of each. Another technique used to reduce interference between power and data signals is time-division multiplexing (TDM) [84], [85]. During the power transfer time slot, the transmitter sends a high-power signal to charge the battery or power the device. During the data transfer time slot, the transmitter sends a low-power signal carrying the data, and the receiver switches to a low-power mode to receive the data.

Multichannel SWIPT (MC-SWIPT) systems, such as those described in [65] and [86], implement separate channels or pairs of coils for power and data transfer, operating independently of each other. Incorporating additional coil sets offers several benefits, including enhanced reliability, increased data transfer rates, improved efficiency, and intrinsic bidirectional data communication. Nevertheless, for certain applications, this approach might become impractical due to the associated size, cost, and system complexity. To address this limitation, Wu et al. [84] proposed a structure with a metal plate added below each coil, as in Fig. 11. Power is transferred through the coil's magnetic field, while data is modulated and transmitted through the metal plate capacitance and the coil's parasitic capacitance. Thus, the addition of metal plates removes the need for extra coils. However, the high electrical permittivity and permeability of the ferrite layer, required for improving the coupling, leads to a significant disturbance caused by the power transfer on the data transmission channel.

**TABLE 1.** State-of-the-art SWIPT systems in the literature.

| Reference | Year | Technique | Operating Frequency [Hz] | Output Power [W] | Peak Efficiency [%] | Transfer Distance [mm] | Data rate [kbps] | Data Transmission Type |
|---|---|---|---|---|---|---|---|---|
| [65] | 2012 | MC-SWIPT | 1M | NA | NA | 30 | NA | NA |
| [43] | 2015 | PC-SWIPT | 13.56M | 102m | 50 | 10 | 500 | Uplink |
| [83] | 2015 | HFDC-SWIPT | 22.4k | 500 | 86 | 75 | 20 | Bidirectional |
| [81] | 2016 | HFDC-SWIPT | 40k | 250 | 83.2 | 7 | 19.2 | Bidirectional |
| [73] | 2017 | PC-SWIPT | 22k | 700 | 87 | 25 | NA | Uplink |
| [88] | 2017 | HFDC-SWIPT | 80k | 30 | NA | 10 | 80 | Bidirectional |
| [89] | 2018 | MC-SWIPT | 40k | 40 | 79.6 | 20 | 230 | Bidirectional |
| [77] | 2019 | PC-SWIPT | 260k/351k | 2.5 | 85 | 50 | 20 | Downlink |
| [68] | 2019 | PC-SWIPT | 1.8M-13.56M | 94m | 80.1 | 42 | 5000 | Uplink |
| [78] | 2019 | PC-SWIPT | 10k-2M | NA | NA | NA | 500 | Downlink |
| [72] | 2019 | HFDC-SWIPT | 85k | 3.3k | NA | NA | 64 | Bidirectional |
| [86] | 2019 | MC-SWIPT | 200k | 122 | 87 | 20 | 19.2 | Uplink |
| [79] | 2020 | PC-SWIPT | 13.56M | 9.2m | 75.4 | NA | 100 | Downlink |
| [56] | 2020 | PC-SWIPT | 13.56M | 10m | 92.6 | 20 | 100 | Downlink |
| [66] | 2020 | PC-SWIPT | 13.56M | 180m | 90.9 | 10 | 211 | Bidirectional |
| [82] | 2021 | HFDC-SWIPT | 85k | 150 | 90 | 30 | 166.7 | Bidirectional |
| [74] | 2021 | PC-SWIPT | 83k | 800 | 72.5 | 20 | NA | Bidirectional |
| [67] | 2021 | PC-SWIPT | 6.5M/7.5M | 115m | 56.7 | 5 | 2500 | Downlink |
| [75] | 2022 | PC-SWIPT | 2M/4M | 140m | 14 | 10 | 800 | Bidirectional |
| [70] | 2023 | PC-SWIPT | 13.56M | 2m | 83.3 | 10 | 1000 | Bidirectional |
| [71] | 2023 | HFDC-SWIPT | 249.2k | 200 | 92.25 | 50 | 30 | Uplink |

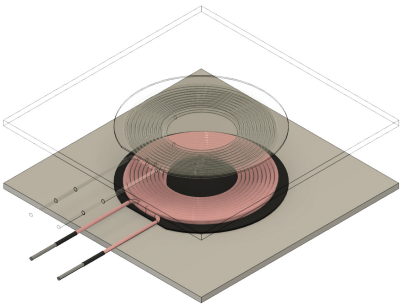

**FIGURE 11.** 3-D view of the structure presented in [84].

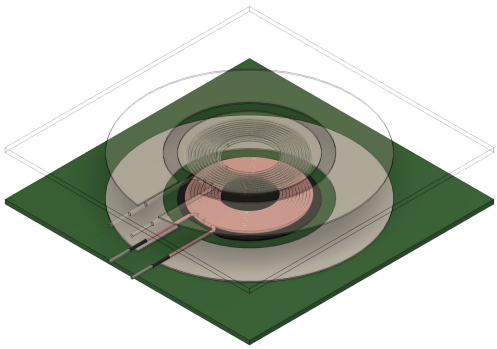

**FIGURE 12.** 3-D view of the structure presented in [87].

A novel capacitive–inductive channel structure presented in [87] enables simultaneous power and data transmission over the same line, without any negative effects from the parasitic capacitance between a metal plate and its adjacent coil. Instead of placing the coil above the metal plate, the coil is encircled by a copper ring printed on the PCB, as shown in Fig. 12, constituting the capacitor plate. This configuration maintains strong coupling between the two metal rings, while considerably reducing the parasitic capacitance that exists between adjacent coils and plates.

Table 1 provides an overview of the state-of-the-art of SWIPT systems, showcasing notable examples from the recent literature. The table summarizes the performance of these systems based on various parameters, including the data transmission technique (PC-SWIPT, HFDC-SWIPT, or MC-SWIPT), selected operating frequency, maximum-achievable output power, peak efficiency, transfer distance between coils, data rate, and data transmission type (uplink, downlink, or bidirectional). The power-carrier-based method is highly preferred due to its ability to achieve data signal modulation directly using the power signal as a carrier, without the need for special structures to inject data or particular multichannel antenna structures. PC-SWIPT systems usually operate at higher frequencies to enhance the data rate, whereas HFDC-SWIPT and MC-SWIPT systems employ lower operating frequencies to prevent interference with the high-frequency data carrier. In PC-SWIPT systems, achieving high efficiency and high data rate is often a tradeoff since data transmission is directly connected to the power signal. In contrast, HFDC-SWIPT and MC-SWIPT systems offer the possibility of obtaining both good power and data

transmission performances but require more complicated structures. Data transmission is typically unidirectional in PC-SWIPT systems. If ASK or FSK modulation is used, data transmission is in the downlink direction, while LSK modulation enables uplink communication. However, bidirectional communication is possible if both techniques are implemented in the same system. On the other hand, HFDC-SWIPT and MC-SWIPT systems are inherently bidirectional, supporting both half-duplex and full-duplex communication. In HFDC-SWIPT systems, the data transmission direction depends on where the data is injected and extracted (TX or RX). Meanwhile, in MC-SWIPT systems, with a more complex transmission structure (e.g., extra coil pairs), the data transmission direction can be arbitrarily determined by the designer.

### D. MULTIPLE-LOADS, MULTIPLE-STANDARDS AND MULTIPLE-DIRECTIONS WPT SYSTEMS

As the issue of WPT between one TX and one RX according to a specified standard has been mostly solved, the interest of research has moved also to solutions implementing WPT to multiple loads, supporting different standards or allowing bidirectional power transfer, i.e., device-to-device charging.

Considering the issue of multiple loads, employing inductive coupling is not a viable possibility as the TX and the RX should be strongly coupled and, therefore, aligned and very close to each other, which is not possible when there are one transmitter and multiple receivers. Magnetic resonance coupling instead supports multiload WPT. Indeed, exploiting separate resonance frequencies for different receivers allows selectively transmitting power to one RX, as each RX features a distinct resonance frequency that constitutes a specific passband: hence, by selecting the corresponding TX frequency and impedance values, only one power link is active at a time [90], [91]. Therefore, by using a time-sharing control strategy, the power distribution among several loads can be realized simply by controlling the duty cycle for each load. The time-sharing control can be implemented, for instance, by selectively turning on/off a controllable resonant capacitor, thus enabling the TX to supply the RX with the corresponding natural resonant frequency [92]. In order to charge multiple loads simultaneously, the frequency splitting phenomenon can be exploited: indeed in [93], it was observed that by designing the load coils frequencies equal to the RX split frequencies, the power flow can become simultaneous and independent of cross interference. When multiple loads are present, cross-coupling effects between the receivers are a non-negligible issue, as they lead to correlation between the output characteristics of each load, while also reducing the WPT system efficiency and power transfer capability [94]. Cross-coupling compensation can be implemented by measuring selected RX parameters and transmitting them to the TX, however this involves requiring and relying on TX–RX communication; another approach, proposed in [94], allows compensating the cross-coupling

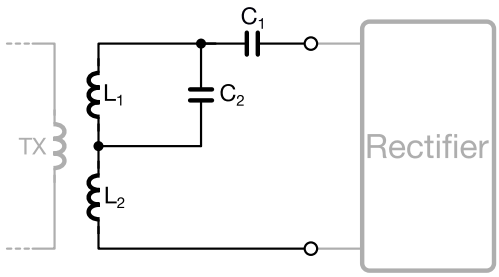


**FIGURE 13.** Schematic representation of an antenna supporting both Qi/PMA and Airfuel standards.

effects adaptively by implementing a closed-loop control based on the phase-shift regulation technique in active rectifiers, thus avoiding the need for communication. Another issue when considering a multiple-loads system is scalability, i.e., ensuring good WPT in the presence of a changing number of loads. This issue was tackled in [95] by implementing class-E rectifiers in the receivers and employing their shunt capacitor as a design parameter to tune the rectifier's input impedance. By coupling this approach with an impedance transformation network in the TX power amplifier, it was possible to naturally deliver and maintain a specific target power for each RX, while also enabling a quasi-constant power amplifier output current over a certain variation range of its load, determined by the changing RX number.

As discussed in Section II, there exist different standards for implementing WPT: together with the already cited Qi and Airfuel standards, an additional inductive-based standard, known as PMA (Power Matters Alliance), also exists. The PMA standard operates in a similar frequency range to Qi, hence supporting both standards is quite easy; the same is not true for supporting Qi/PMA and Airfuel, since their frequencies differ for more than one order of magnitude. Nevertheless, many solutions have been implemented supporting the different employed standards: this interest arises from the desire to not be standard-dependent and be instead able to achieve WPT in every situation. Cross-standard compatibility was achieved for the TX in [96] using the adaptive gate splitting technique and free-wheeling control in the power amplifier, whose programmable power supply was supplied from high-efficiency dc–dc converters and whose output power was controlled through the RX–TX communication, according to the required different protocols. Multiple-standard receivers were presented in [97], [98], [99], [100], [101], and [102]. The easiest solution to cover the three standards is using two antennas (one for Qi/PMA and one for Airfuel) and two rectifiers, however, this would lead to increased area and power losses, since undesired magnetic coupling would still be present and could activate both rectifiers: for these reasons, it is preferred to use only one rectifier and two antennas [99]. Employing two separate antennas is desired as it enables independent selection of inductance value and $Q$-factor, thus maximizing

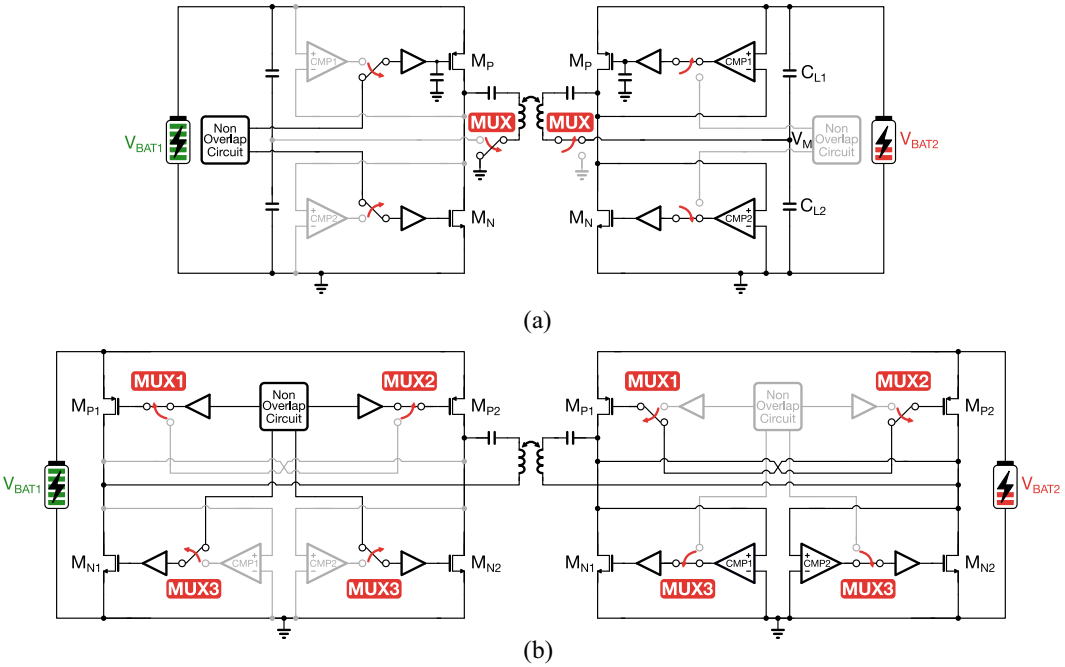


**FIGURE 14.** Schematic representation of the main TX–RX reconfigurable topologies for bidirectional WPT systems: (a) transceiver that can act as an active voltage doubler or as a single-ended power amplifier and (b) transceiver reconfigurable as a differential class-D power amplifier or as a full-wave active rectifier.

efficiency at both frequency ranges. The two antennas can actually be merged together in a single structure [97], [101], as illustrated in Fig. 13, which creates two series resonances, one at low frequency (for Qi/PMA, i.e., 100–300 kHz, given by $L_1 + L_2$ and $C_1$) and one at high frequency (for Airfuel, i.e., 6.78 MHz or its multiples, given by $L_2$ and $C_2$). Indeed at low frequency, capacitor $C_2$ can be approximated as an open circuit, while at high frequency, the large $C_1$ capacitor acts as a short circuit and the impedance of $L_1$ is very large compared to the one of $C_2$. In this way, inductor $L_1$ is optimized for operation in the Qi/PMA frequency range, while inductor $L_2$ is optimized for operation at the Airfuel frequency; while capacitors $C_1$ and $C_2$ are selected accordingly for implementing the two desired resonance frequencies.

Together with supporting multiple standards, the need for implementing bidirectional WPT has arisen, with the goal of enabling device-to-device charging, e.g., for allowing a mobile phone to charge another mobile or wearable device [100], [107], [108], [109]. In order to support bidirectional WPT, the device needs to be able to act both as an RX and as a TX: hence, the rectifier needs to be reconfigurable as a power amplifier with limited area overhead. Two different reconfigurable transceiver topologies are illustrated in Fig. 14 [108]. The first topology, reported in Fig. 14(a), features a transceiver that can act as an active voltage doubler or as a single-ended power amplifier. This topology suffers from several drawbacks. It features a significant increase in silicon area as *MUX* needs to be an nMOS with the same size as $M_N$ in the TX mode and it needs to feature both an nMOS and a pMOS in RX mode since the $V_M$ voltage is approximately equal to half $V_{BAT2}$; in addition, two extra capacitors ($C_{L1}$ and $C_{L2}$) are required. *MUX* generates additional conduction losses, thus negatively affecting the system efficiency and the single-ended power amplifier output peak-to-peak amplitude reaches only the source battery voltage, which results in a low output power. The second topology, instead, illustrated in Fig. 14(b), implements a bidirectional transceiver reconfigurable as a differential class-D power amplifier or as a full-wave active rectifier. It consists of four power devices ($M_{N1} - M_{N2}$, $M_{P1} - M_{P2}$) and four multiplexers ($MUX1 - MUX4$). In the TX mode, the multiplexers connect the power device gates to the nonoverlapping gate drivers, while in the RX mode, $M_{P1} - M_{P2}$ are cross-connected and $M_{N1} - M_{N2}$ are controlled as active diodes by $CMP1 - CMP2$: in this way, the multiplexers are not on the power path since they only deal with gate control signals and, therefore, can be small-sized and constitute negligible area overhead. Hence, this topology consisting of a reconfigurable cross-connected transceiver is the preferred one [107], [108], [109]. Since, differently from traditional WPT, the device-to-device charging draws the power from an energy-constrained battery, achieving very high efficiency is of paramount importance: this can be obtained thanks to appropriate switch timing control techniques [107], such as delay-locked loops realizing an adaptive deadtime control in the TX mode and an off-delay compensation in the RX mode [109]. Furthermore, the number of stages needs to be minimized in order not to decrease the efficiency: hence the rectifier is usually employed for directly charging the load at maximum current since the limited power capability of the

**TABLE 2.** State-of-the-art complete WPT systems in the literature.

| Works | Year | WPT Technology | Operating Frequency [Hz] | Output Power [W] | Peak Efficiency [%] | d [mm] | D (TX, RX) [mm] |
|---|---|---|---|---|---|---|---|
| [17] | 2013 | Res | 6.78M | 6 | 55 | NA | NA |
| [7] | 2013 | Res | 9M | 100m | 33 | 30 | 7 (RX) |
| [4] | 2013 | Ind | 20k | 100k | 80 | 260 | NA |
| [43] | 2015 | Res | 13.56M | 102m | 50 | 3 | 25, 9.5 |
| [103] | 2015 | Ind | 60k | 1M | 82.7 | 100 | NA |
| [83] | 2015 | Ind | 22.4k | 500 | NA | 100 | 75, 75 |
| [104] | 2015 | Res | 2M | 1.45 | 27 | 80 | 140, 65 |
| [105] | 2015 | Res | 50.95k | 420 | 89 | 200 | NA |
| [81] | 2016 | Ind | <100k | 50-250 | 86 | 2-7 | NA |
| [13] | 2016 | Ind+Cap | 1M | 2.84k | 94.5 | NA (k=0.13) | 610, 456 |
| [42] | 2017 | Res | 6.78M | 600m | 42.1 | 5 | 24, 16 |
| [73] | 2017 | Ind | 22k | 700k | 87 | 20 | 165, 165 |
| [88] | 2017 | Ind | 80k | 30 | NA | 10 | NA |
| [106] | 2018 | Res | 585k | 3 | 81 | NA | NA |
| [101] | 2018 | Res/Ind | 6.78M/85k-500k | 9 | 84.5/85.5 | NA | NA |
| [40] | 2018 | Res | 13.56M | 49.4m | 70.6 | 6 | 25, 20 |
| [107] | 2018 | Res (Bi) | 6.78M | 2.7 | 78.1 | 23 | 40, 40 |
| [108] | 2019 | Res (Bi) | 6.78M | 1.6 | 58.6 | NA (k=0.3) | 33, 33 |
| [72] | 2019 | Ind | 85k | 3.3k | NA | NA (k=0.184) | NA |
| [86] | 2019 | Ind | 200k | 122 | 87 | NA | 100, 100 |
| [109] | 2019 | Res (Bi) | 6.78M | 2.74 | 77.2 | 24 | 40, 40 |
| [110] | 2020 | Ind | 88k | 50k | 95 | 150 | 544 |
| [79] | 2020 | Res | 13.56M | 9.2m | 75.4 | NA | 22, 22 |
| [111] | 2020 | Ind+Cap | 1M | 653 | 87.7 | NA | 600, 600 |
| [112] | 2020 | Res | 294k | 400 | 91.9 | 150 | 300, 300 |
| [66] | 2020 | Res | 13.56M | 180m | 44.8 | NA | NA |
| [41] | 2020 | Res | 6.78M/13.56M | 2/1.5 | 71 | 20 | 100, 100 |
| [102] | 2021 | Res/Ind | 6.78M/85k-500k | 15 | 92.3/95.3 | NA | NA |
| [44] | 2021 | Res | 6.78M | 400m | 71.5 | 3 | 45, 45 |
| [74] | 2021 | Ind | 83k | 800 | 72.5 | 25 | 200, 200 |
| [113] | 2021 | Res | 6.78M | 45.7 | 85.5 | 30 | 94, 35 |
| [67] | 2021 | Res | 6.5M-7.5M | 115m | 56.7 | 5 | 30, 30 |
| [75] | 2022 | Ind | 2M-4M | 140m | 14 | 10 | 35, 20 |
| [45] | 2022 | Res | 13.56M | 70m | 70.1 | 1 | 30, 22 |
| [35] | 2023 | Res/Ind | 6.78M/87k-357k | 7 | 86.7/88.2 | NA | NA |
| [47] | 2023 | Res | 6.78M | 900m | 77 | 20 | NA |
| [114] | 2023 | Res | 200k | 700 | 90 | NA | NA |
| [115] | 2023 | Res | 13.56M | 150m | 60-5 | 30-185 | 150, 86 |

source ensures that the maximum current rating can hardly be reached [100], [108].

## IV. STATE-OF-THE-ART OVERVIEW

In order to identify the current and future research trends, an overview of the state-of-the-art of WPT systems is presented. Table 2 gathers the main complete RX–TX WPT systems examples presented in the literature in the last ten years: the type of employed WPT technology (inductive - *Ind*, resonant - *Res* or capacitive - *Cap*), the selected operating frequency, the maximum achievable output power, the peak efficiency, the distance between coils $d$ (or the coupling coefficient $k$) and the coil diameter $D$ are considered as parameters to summarize the performance of the reported WPT systems.

By examining Table 2, a main trend concerning the type of employed WPT technology can be identified: although at the beginning, the research interest was more focused on inductive solutions, in the last few years, the focus has moved significantly toward magnetic resonance-based (i.e., resonant) systems. This is due to the fact that it is desired to limit the negative effects caused by misalignments: hence, a solution that can work well also with lower coupling coefficients

**TABLE 3.** State-of-the-art WPT receivers in the literature.

| Works | Year | WPT Technology | Operating Frequency [Hz] | Output Power [W] | Peak Efficiency [%] | Notes |
|---|---|---|---|---|---|---|
| [17] | 2013 | Res | 6.78M | 6 | 86 | Regulating rectifier (3 switches) |
| [53] | 2013 | Ind | 100k-150k | NA | 82 | Resonant capacitor-free rectifier |
| [26] | 2014 | Res | 13.56M | 24.8m | 90.1 | Active rectifier with delay compensation |
| [38] | 2014 | Res | 13.56M | 40m | 85 | Voltage doubler active rectifier |
| [43] | 2015 | Res | 13.56M | 102m | 92.6 | Regulating rectifier (1x-2x) |
| [97] | 2015 | Res/Ind | 6.78M/100k-200k | 5 | 83/85 | Multi-mode RX |
| [104] | 2015 | Res | 2M | 1.45 | 76 | Regulating rectifier (1 switch) |
| [33] | 2016 | Res | 6.78M | 6 | 80.7 | Active rectifier with DDL-based delay compensation + DC DC |
| [31] | 2016 | Res | 13.56M | 64.8m | 91.4 | Active rectifier with on/off delay compensation |
| [25] | 2016 | Res | 6.78M | 6 | 92.2 | Regulating rectifier (1x-0.5x-0x) |
| [42] | 2017 | Res | 6.78M | 600m | 80.5 | Voltage doubler active rectifier |
| [101] | 2018 | Res/Ind | 6.78M/85k-500k | 9 | 91.7/92.7 | Multi-mode RX |
| [27] | 2018 | Res | 13.56M | 89m | 91.9 | Active rectifier with dynamically controllable common-gate comparators |
| [108] | 2019 | Res (Bi) | 6.78M | 1.6 | 91.5 | Reconfigurable active rectifier |
| [32] | 2019 | Res | 13.56M | 10.6m | 94.1 | Active rectifier with current-controlled delay compensation |
| [117] | 2019 | Res | 6.78M | 61 | 92 | GaN-based active rectifier |
| [14] | 2020 | Cap | 1M-10M | 232m | 91.5 | Active rectifier with dual-loop delay compensation |
| [59] | 2020 | Res | 6.78M | 6.3 | 92.3 | Regulating rectifier (1x-0.5x-0x) + Constant-current constant-voltage charging |
| [28] | 2020 | Res | 40.68M | 9m | 93.2 | Active rectifier with on/off delay compensation |
| [29] | 2020 | Res | 13.56M | 54m | 92.6 | Active rectifier with SAR-assisted delay compensation |
| [56] | 2020 | Res | 13.56M | 10.9m | 92.6 | Current-based multi-cycling receiver |
| [50] | 2020 | Res | 1M-10M | 65m | 90.7 | Regulating rectifier (PWM+dual-mode PFM) |
| [52] | 2021 | Res | 6.78M | 1.98 | 92.1 | Regulating rectifier (hysteretic control and current wave modulation) |
| [118] | 2021 | Res | 6.78M | 288m | 93.7 | Active rectifier with delay compensation |
| [30] | 2022 | Res | 6.78M | 15m | 95.4 | Active rectifier with hybrid mode delay compensation |
| [34] | 2022 | Res/Ind | 6.78M/150k | 15 | 94.5/98.6 | Active rectifier with gate charge recycling |
| [24] | 2022 | Res | 40.68M | 11.7m | 93.3 | Active rectifier with inverter-base conduction time generator |
| [70] | 2023 | Res | 13.56M | 2m | 75 | Active rectifier + LDO |
| [51] | 2023 | Res | 6.78M | 79.8m | 90.6 | Voltage doubler regulating rectifier |

is preferable. Furthermore, higher operating frequencies in the MHz range, as the ones employed in magnetic resonance-based solutions, enable the use of smaller size coils, e.g., as low as 7 mm in [7], [116], thus catering to the needs of wearable and implantable devices, which are becoming also a hot topic in recent years. Typical coil sizes fall within the 15–100-mm range, however, they can also be significantly larger, e.g. >300 mm [13], [111], [112], especially when large output power levels are desired.

In order to better appreciate the relationship between the type of near-field WPT technology, output power, efficiency, and selected operating frequency, the works summarized in Table 3 are also illustrated graphically in Figs. 15 and 16, that show the peak efficiency and the operating frequency, respectively, as a function of the output power level. From Fig. 15, it is evident how the desired output power target tends to determine the choice of WPT technology: indeed, for high output power levels (>1 kW), inductive-based systems are preferred, whereas for low power levels (<1 W), resonant technology constitutes the go-to solution. When a mid-range output power, between 1 W and 1 kW, is required, both the inductive and the resonant technologies, as well as hybrid inductive–capacitive solutions, can be employed. This division is due to the fact that resonant systems pay a penalty in terms of efficiency with respect to inductive solutions: hence, they are not well suited to cases where large power levels and, therefore, large losses, resulting in significant self-heating issues, are involved. Instead, resonant solutions

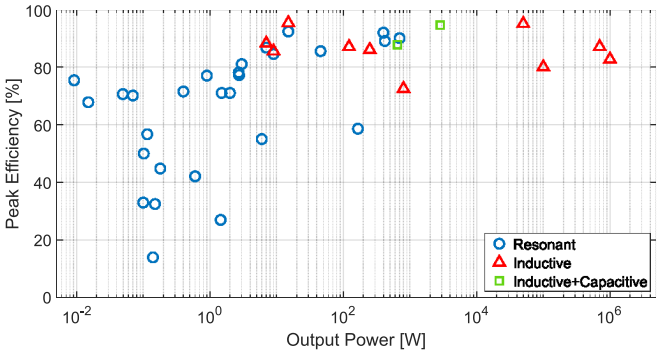


**FIGURE 15.** Graphical representation of the works summarized in Table 2, where the peak efficiency and the output power are reported on the *y*-axis and *x*-axis, respectively.

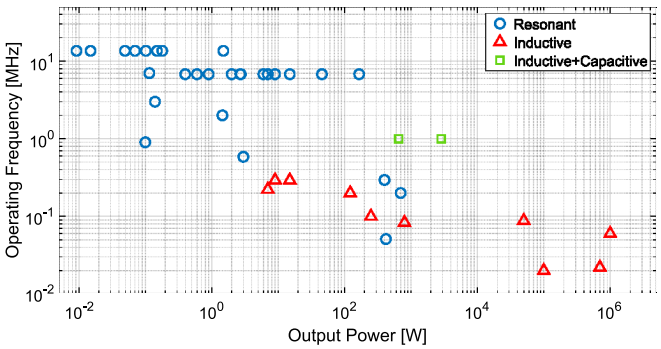


**FIGURE 16.** Graphical representation of the works summarized in Table 2, where the operating frequency and the output power are reported on the *y*-axis and *x*-axis, respectively.

excel for low-power systems, that typically imply miniaturization, as they enable the employment of small inductors. When mid-range power levels are considered, addressing power requirements for mobile devices, tablets, laptops, and consumer electronic devices in general, both inductive and resonant technologies can be employed, depending on the most critical system requirements: inductive solutions enable very high efficiency, whereas resonant solutions allow more spatial freedom as well as single-TX multiple-RX configurations. Concerning the selection of the operating frequency, Fig. 16 stresses how the inductive technology allows much more freedom with respect to the resonant one, where most selected frequencies are 6.78 MHz and its multiples. Indeed, although it is also possible to design a custom resonant system, most solutions in the literature target instead the Airfuel standard.

It is important to notice how the total achieved system peak efficiency can be rather low (<60%) in resonant solutions, not only for very low power cases but also when Watts are involved: this is due to the fact that in the overall system, many stages (TX, Antenna, and RX, which can in turn include different blocks) are cascaded and, therefore, the total efficiency is given by the product of the efficiency of the different blocks. In order to improve the overall system efficiency, therefore, it is very important to maximize the efficiency of every single stage. Research in the last few years has focused in particular on the receiver and, more specifically, on the active rectifier block, with the aim of achieving peak efficiency well exceeding 90%.

Table 3 summarizes the RX state-of-the-art in terms of the type of WPT technology, operating frequency, output power, and peak efficiency. Moreover, the table also highlights the proposed circuit's peculiarities, thus allowing to identify the main research design trends. As expected, given the interest in overall resonant WPT systems, the research interest has focused almost exclusively on resonant solutions. Two main research areas, both targeting efficiency enhancements, can be identified: 1) delay-compensated active rectifiers and 2) regulating rectifiers. The interest in delay-compensated structures [26], [27], [28], [29], [30], [31], [32], [33], [59], [118] stems from the necessity to optimize the functioning of standard active rectifiers: indeed, by compensating the delay times, unwanted currents flowing during the switches operation, and hence unwanted losses, are avoided. Delay compensation is particularly critical in resonant systems as they feature typically high frequency, in the MHz range, and are therefore more sensitive to timing errors. The other main trend, i.e., regulating rectifiers (including voltage doubler rectifiers [38], [42], [51]), arises from the desire to minimize the number of cascaded blocks: indeed by combining together as many stages as possible (e.g., rectifiers and regulators [17], [25], [43], [50], [52], [104] or rectifiers, regulator and battery charger circuit [25], [59]) the overall system efficiency can be improved.

By analyzing the RX WPT system state-of-the-art, the other main challenges discussed in Section III, i.e., multimode RX supporting both inductive and resonant standards [97], [101] and reconfigurable rectifiers enabling bidirectional (Bi) operation [108], can be identified as well. As for the overall system case, different power levels are tackled (from mW to tens of Watts): the majority of works however target low power, mostly biomedical, solutions with high operating frequencies (13.56 MHz or even 40.68 MHz).

Rectifier and receiver efficiency values well exceeding 90% are achieved; however, when considering the overall system efficiency, a significant decrease can be observed, e.g., in [17], [42], [43], [101], [104], and [108]. This decrease is mostly due to the TX power amplifier [108] or to the antenna [42], [104]. In [108], however, the power amplifier is implemented through a reconfigurable rectifier; thus, it is not optimized exclusively for the TX operation. Hence, it is the antenna that generally constitutes the limiting factor; for this reason, investigations on how to improve the antenna itself are being carried out: for example, metamaterial slabs can be employed for focusing the magnetic field between TX and RX, thus improving the power transfer efficiency despite misalignment issues [104], [119], [120], [121].

## V. CONCLUSION

WPT systems are becoming more and more pervasive in today's world as they can be employed in a wide range

of applications, from electric vehicles and industrial applications, to healthcare devices, consumer electronics, and many more. This article has provided a general overview of the available WPT technologies, focusing in particular on near-field implementations, and has delved into the main different challenges encountered in the design of near-field WPT systems while illustrating the proposed solutions in the literature. The main critical challenges have been identified as the rectifier circuit, the regulation, and the support of multiple standards, loads, or power transfer directions in the same system. Furthermore, a summary of the state-of-the-art was provided considering WPT system solutions proposed in the last ten years, thus identifying the main trends for the future, which include the focus on magnetic resonance-based systems, the desire to minimize the number of cascaded stages, and the need to address very different power levels, depending on the application.

## REFERENCES


[1] L. Yang et al., "Analysis and design of four-plate capacitive wireless power transfer system for undersea applications," *CES Trans. Electr. Mach. Syst.*, vol. 5, no. 3, pp. 202–211, Sep. 2021.

[2] A. Kosuge et al., "An inductively powered wireless solid-state drive system with merged error correction of high-speed wireless data links and NAND flash memories," *IEEE J. Solid-State Circuits*, vol. 51, no. 4, pp. 1041–1050, Apr. 2016.

[3] S. Y. Hui, "Planar wireless charging technology for portable electronic products and Qi," *Proc. IEEE*, vol. 101, no. 6, pp. 1290–1301, Jun. 2013.

[4] J. Shin et al., "Design and implementation of shaped magnetic-resonance-based wireless power transfer system for roadway-powered moving electric vehicles," *IEEE Trans. Ind. Electron.*, vol. 61, no. 3, pp. 1179–1192, Mar. 2014.

[5] M. Dautta, A. Jimenez, K. K. H. Dia, N. Rashid, M. A. Al Faruque, and P. Tseng, "Wireless Qi-powered, multinodal and multisensory body area network for mobile health," *IEEE Internet Things J.*, vol. 8, no. 9, pp. 7600–7609, May 2021.

[6] M. Wagih, A. Komolafe, and B. Zaghari, "Dual-receiver wearable 6.78 MHz resonant inductive wireless power transfer glove using embroidered textile coils," *IEEE Access*, vol. 8, pp. 24630–24642, 2020.

[7] X. Zhang, S. L. Ho, and W. N. Fu, "A hybrid optimal design strategy of wireless magnetic-resonant charger for deep brain stimulation devices," *IEEE Trans. Magn.*, vol. 49, no. 5, pp. 2145–2148, May 2013.

[8] S. Roy, A. N. M. W. Azad, S. Baidya, M. K. Alam, and F. Khan, "Powering solutions for biomedical sensors and implants inside the human body: A comprehensive review on energy harvesting units, energy storage, and wireless power transfer techniques," *IEEE Trans. Power Electron.*, vol. 37, no. 10, pp. 12237–12263, Oct. 2022.

[9] X. Lu, P. Wang, D. Niyato, D. I. Kim, and Z. Han, "Wireless charging technologies: Fundamentals, standards, and network applications," *IEEE Commun. Surveys Tuts.*, vol. 18, no. 2, pp. 1413–1452, 2nd Quart., 2016.

[10] R. Zhang and C. K. Ho, "MIMO broadcasting for simultaneous wireless information and power transfer," *IEEE Trans. Wireless Commun.*, vol. 12, no. 5, pp. 1989–2001, May 2013.

[11] C. S. Branch. "Limits of human exposure to radiofrequency electromagnetic energy in the frequency range from 3 kHz to 300 GHz." 2009. Accessed: Aug. 7, 2023. [Online]. Available: http://collectiveactionquebec.com/uploads/8/0/9/7/80976394/exhibit_r-65_safety_code_6_2015.pdf

[12] G. Roberts et al., "A contactless transfer device for power and data," in *Proc. IEEE Aerosp. Appl. Conf. Proc.*, vol. 2, 1996, pp. 333–345.

[13] F. Lu, H. Zhang, H. Hofmann, and C. C. Mi, "An inductive and capacitive combined wireless power transfer system with LC-compensated topology," *IEEE Trans. Power Electron.*, vol. 31, no. 12, pp. 8471–8482, Dec. 2016.

[14] R. Erfani, F. Marefat, S. Nag, and P. Mohseni, "A 1–10-MHz frequency-aware CMOS active rectifier with dual-loop adaptive delay compensation and >230-mW output power for capacitively powered biomedical implants," *IEEE J. Solid-State Circuits*, vol. 55, no. 3, pp. 756–766, Mar. 2020.

[15] E. Abramov and M. M. Peretz, "Multi-loop control for power transfer regulation in capacitive wireless systems by means of variable matching networks," *IEEE J. Emerg. Sel. Topics Power Electron.*, vol. 8, no. 3, pp. 2095–2110, Sep. 2020.

[16] J. Dai and D. C. Ludois, "A survey of wireless power transfer and a critical comparison of inductive and capacitive coupling for small gap applications," *IEEE Trans. Power Electron.*, vol. 30, no. 11, pp. 6017–6029, Nov. 2015.

[17] J.-H. Choi, S.-K. Yeo, S. Park, J.-S. Lee, and G.-H. Cho, "Resonant regulating rectifiers (3R) operating for 6.78 MHz resonant wireless power transfer (RWPT)," *IEEE J. Solid-State Circuits*, vol. 48, no. 12, pp. 2989–3001, Dec. 2013.

[18] "Airfuel alliance." Accessed: May 7, 2023. [Online]. Available: https://airfuel.org/airfuel-resonant/

[19] M. Meng and M. Kiani, "A hybrid inductive-ultrasonic link for wireless power transmission to millimeter-sized biomedical implants," *IEEE Trans. Circuits Syst. II, Exp. Briefs*, vol. 64, no. 10, pp. 1137–1141, Oct. 2017.

[20] Y.-C. Lin, M.-C. Chiang, and J.-H. Chen, "A wireless sensor utilizing ultrasound for wireless power and data transmission," in *Proc. IEEE Wireless Power Transfer Conf. (WPTC)*, 2017, pp. 1–3.

[21] X. Yi, W. Zheng, H. Cao, S. Wang, X. Feng, and Z. Yang, "Wireless power transmission for implantable medical devices using focused ultrasound and a Miniaturized 1-3 piezoelectric composite receiving transducer," *IEEE Trans. Ultrason., Ferroelectr., Freq. Control*, vol. 68, no. 12, pp. 3592–3598, Dec. 2021.

[22] Q. Liu et al., "Charging unplugged: Will distributed laser charging for mobile wireless power transfer work?" *IEEE Veh. Technol. Mag.*, vol. 11, no. 4, pp. 36–45, Dec. 2016.

[23] Q. Sheng et al., "Adaptive wireless power transfer via resonant laser beam over large dynamic range," *IEEE Internet Things J.*, vol. 10, no. 10, pp. 8865–8877, May 2023.

[24] Q. Duan, C. Chen, X. Han, and L. Cheng, "A 40.68-MHz active rectifier using an inverter-based conduction-time generator for wirelessly powered implantable medical devices," *IEEE Trans. Circuits Syst. II, Exp. Briefs*, vol. 69, no. 11, pp. 4334–4338, Nov. 2022.

[25] L. Cheng, W.-H. Ki, and C.-Y. Tsui, "A 6.78-MHz single-stage wireless power receiver using a 3-mode reconfigurable resonant regulating rectifier," *IEEE J. Solid-State Circuits*, vol. 52, no. 5, pp. 1412–1423, May 2017.

[26] Y. Lu and W.-H. Ki, "A 13.56 MHz CMOS active rectifier with switched-offset and compensated biasing for biomedical wireless power transfer systems," *IEEE Trans. Biomed. Circuits Syst.*, vol. 8, no. 3, pp. 334–344, Jun. 2014.

[27] H.-C. Cheng, C.-S. A. Gong, and S.-K. Kao, "A 13.56 MHz CMOS high-efficiency active rectifier with dynamically controllable comparator for biomedical wireless power transfer systems," *IEEE Access*, vol. 6, pp. 49979–49989, 2018.

[28] S. Pal and W.-H. Ki, "40.68 MHz digital on-off delay-compensated active rectifier for WPT of biomedical applications," *IEEE Trans. Circuits Syst. II, Exp. Briefs*, vol. 67, no. 12, pp. 3307–3311, Dec. 2020.

[29] Y. Ma, K. Cui, Z. Ye, Y. Sun, and X. Fan, "A 13.56-MHz active rectifier with SAR-assisted coarse-fine adaptive digital delay compensation for biomedical implantable devices," *IEEE Solid-State Circuits Lett.*, vol. 3, pp. 122–125, 2020.

[30] K. S. Zheng, X. Liu, X. Wang, Q. Su, and Y. Liu, "A 6.78 MHz CMOS active rectifier with hybrid mode delay compensation for wireless power transfer systems," *IEEE Access*, vol. 10, pp. 46176–46186, 2022.

[31] L. Cheng, W.-H. Ki, Y. Lu, and T.-S. Yim, "Adaptive on/off delay-compensated active rectifiers for wireless power transfer systems," *IEEE J. Solid-State Circuits*, vol. 51, no. 3, pp. 712–723, Mar. 2016.

[32] Z. Xue, S. Fan, D. Li, L. Zhang, W. Gou, and L. Geng, "A 13.56 MHz, 94.1% peak efficiency CMOS active rectifier with adaptive delay time control for wireless power transmission systems," *IEEE J. Solid-State Circuits*, vol. 54, no. 6, pp. 1744–1754, Jun. 2019.

[33] H.-G. Park et al., "A design of a wireless power receiving unit with a high-efficiency 6.78-MHz active rectifier using shared DLLs for magnetic-resonant A4 WP applications," *IEEE Trans. Power Electron.*, vol. 31, no. 6, pp. 4484–4498, Jun. 2016.

[34] Q. U. Ain et al., "A high-efficiency triple-mode active rectifier with gate charge recycling technique for wireless power transfer system," *IEEE Access*, vol. 10, pp. 45943–45953, 2022.

[35] S. A. A. Shah et al., "A design of wireless power receiver with gate charge recycled dual-mode active rectifier and step-down converter with 88.2% system efficiency for power management IC," *IEEE Trans. Power Electron.*, vol. 38, no. 1, pp. 1348–1360, Jan. 2023.

[36] Z. Liu, Z. Zhong, and Y.-X. Guo, "A reconfigurable diode topology for wireless power transfer with a wide power range," *IEEE Microw. Wireless Compon. Lett.*, vol. 26, no. 10, pp. 846–848, Oct. 2016.

[37] M. Fu, C. Ma, and X. Zhu, "A cascaded boost–buck converter for high-efficiency wireless power transfer systems," *IEEE Trans. Ind. Informat.*, vol. 10, no. 3, pp. 1972–1980, Aug. 2014.

[38] C.-Y. Wu, X.-H. Qian, M.-S. Cheng, Y.-A. Liang, and W.-M. Chen, "A 13.56 MHz 40 mW CMOS high-efficiency inductive link power supply utilizing on-chip delay-compensated voltage doubler rectifier and multiple LDOs for implantable medical devices," *IEEE J. Solid-State Circuits*, vol. 49, no. 11, pp. 2397–2407, Nov. 2014.

[39] A. Berger, M. Agostinelli, S. Vesti, J. A. Oliver, J. A. Cobos, and M. Huemer, "A wireless charging system applying phase-shift and amplitude control to maximize efficiency and extractable power," *IEEE Trans. Power Electron.*, vol. 30, no. 11, pp. 6338–6348, Nov. 2015.

[40] C. Huang, T. Kawajiri, and H. Ishikuro, "A 13.56-MHz wireless power transfer system with enhanced load-transient response and efficiency by fully integrated wireless constant-idle-time control for biomedical implants," *IEEE J. Solid-State Circuits*, vol. 53, no. 2, pp. 538–551, Feb. 2018.

[41] M.-L. Kung and K.-H. Lin, "A dual-band wireless power transfer system with efficiency-boosting converter," *IEEE Microw. Wireless Compon. Lett.*, vol. 30, no. 11, pp. 1108–1111, Nov. 2020.

[42] Y. Lu, M. Huang, L. Cheng, W.-H. Ki, U. Seng-Pan, and R. P. Martins, "A dual-output wireless power transfer system with active rectifier and three-level operation," *IEEE Trans. Power Electron.*, vol. 32, no. 2, pp. 927–930, Feb. 2017.

[43] X. Li, C.-Y. Tsui, and W.-H. Ki, "A 13.56 MHz wireless power transfer system with reconfigurable resonant regulating rectifier and wireless power control for Implantable medical devices," *IEEE J. Solid-State Circuits*, vol. 50, no. 4, pp. 978–989, Apr. 2015.

[44] F.-B. Yang, J. Fuh, Y.-H. Li, M. Takamiya, and P.-H. Chen, "Structure-reconfigurable power amplifier (SR-PA) and 0X/1X regulating rectifier for adaptive power control in wireless power transfer system," *IEEE J. Solid-State Circuits*, vol. 56, no. 7, pp. 2054–2064, Jul. 2021.

[45] G. Namgoong, W. Park, and F. Bien, "A 13.56 MHz wireless power transfer system with fully integrated PLL-based frequency-regulated reconfigurable duty control for implantable medical devices," *IEEE Trans. Biomed. Circuits Syst.*, vol. 16, no. 6, pp. 1116–1128, Dec. 2022.

[46] K. Colak, E. Asa, M. Bojarski, D. Czarkowski, and O. C. Onar, "A novel phase-shift control of semibridgeless active rectifier for wireless power transfer," *IEEE Trans. Power Electron.*, vol. 30, no. 11, pp. 6288–6297, Nov. 2015.

[47] X. Bai, Y. Lu, C. Zhan, and R. P. Martins, "A 6.78-MHz wireless power transfer system with inherent wireless phase shift control without feedback data sensing coil," *IEEE J. Solid-State Circuits*, vol. 58, no. 6, pp. 1746–1757, Jun. 2023.

[48] H. S. Gougheri and M. Kiani, "Self-regulated reconfigurable voltage/current-mode inductive power management," *IEEE J. Solid-State Circuits*, vol. 52, no. 11, pp. 3056–3070, Nov. 2017.

[49] C. Kim, S. Ha, J. Park, A. Akinin, P. P. Mercier, and G. Cauwenberghs, "A 144-MHz fully integrated resonant regulating rectifier with hybrid pulse modulation for mm-sized implants," *IEEE J. Solid-State Circuits*, vol. 52, no. 11, pp. 3043–3055, Nov. 2017.

[50] R. Erfani, F. Marefat, and P. Mohseni, "A dual-output single-stage regulating rectifier with PWM and dual-mode PFM control for wireless powering of biomedical implants," *IEEE Trans. Biomed. Circuits Syst.*, vol. 14, no. 6, pp. 1195–1206, Dec. 2020.

[51] T. Lu and S. Du, "A single-stage regulating voltage-doubling rectifier for wireless power transfer," *IEEE Solid-State Circuits Lett.*, vol. 6, pp. 29–32, 2023.

[52] J. Lin, C. Zhan, and Y. Lu, "A 6.78-MHz single-stage wireless power receiver with ultrafast transient response using hysteretic control and multilevel current-wave modulation," *IEEE Trans. Power Electron.*, vol. 36, no. 9, pp. 9918–9926, Sep. 2021.

[53] O. Lazaro and G. A. Rincón-Mora, "180-nm CMOS wideband capacitor-free inductively coupled power receiver and charger," *IEEE J. Solid-State Circuits*, vol. 48, no. 11, pp. 2839–2849, Nov. 2013.

[54] H. S. Gougheri and M. Kiani, "Current-based resonant power delivery with multi-cycle switching for extended-range inductive power transmission," *IEEE Trans. Circuits Syst. I, Reg. Papers*, vol. 63, no. 9, pp. 1543–1552, Sep. 2016.

[55] M. Choi, T. Jang, J. Jeong, S. Jeong, D. Blaauw, and D. Sylvester, "A resonant current-mode wireless power receiver and battery charger with –32 dBm sensitivity for implantable systems," *IEEE J. Solid-State Circuits*, vol. 51, no. 12, pp. 2880–2892, Dec. 2016.

[56] S.-W. Hong, "A resonant current-mode wireless power and data receiver for loosely coupled implantable devices," *IEEE J. Solid-State Circuits*, vol. 55, no. 12, pp. 3200–3209, Dec. 2020.

[57] S.-U. Shin et al., "A 13.56MHz time-interleaved resonant-voltage-mode wireless-power receiver with isolated resonator and quasi-resonant boost converter for implantable systems," in *Proc. IEEE Int. Solid-State Circuits Conf. (ISSCC)*, 2018, pp. 154–156.

[58] Z. Huang, S.-C. Wong, and C. K. Tse, "Design of a single-stage inductive-power-transfer converter for efficient EV battery charging," *IEEE Trans. Veh. Technol.*, vol. 66, no. 7, pp. 5808–5821, Jul. 2017.

[59] L. Cheng et al., "A 6.78-MHz single-stage wireless charger with constant-current constant-voltage charging technique," *IEEE J. Solid-State Circuits*, vol. 55, no. 4, pp. 999–1010, Apr. 2020.

[60] T.-D. Yeo, D. Kwon, S.-T. Khang, and J.-W. Yu, "Design of maximum efficiency tracking control scheme for closed-loop wireless power charging system employing series resonant tank," *IEEE Trans. Power Electron.*, vol. 32, no. 1, pp. 471–478, Jan. 2017.

[61] M. Carbajal-Retana et al., "Interleaved buck converter for inductive wireless power transfer in DC–DC converters," *Electronics*, vol. 9, no. 6, p. 949, 2020.

[62] H. Pinheiro, P. Jain, and G. Joos, "Self-sustained oscillating resonant converters operating above the resonant frequency," *IEEE Trans. Power Electron.*, vol. 14, no. 5, pp. 803–815, Sep. 1999.

[63] W.-Q. Niu, J.-X. Chu, W. Gu, and A.-D. Shen, "Exact analysis of frequency splitting phenomena of contactless power transfer systems," *IEEE Trans. Circuits Syst. I, Reg. Papers*, vol. 60, no. 6, pp. 1670–1677, Jun. 2013.

[64] F. Mastri, A. Costanzo, and M. Mongiardo, "Coupling-independent wireless power transfer," *IEEE Microw. Wireless Compon. Lett.*, vol. 26, no. 3, pp. 222–224, Mar. 2016.

[65] G. Wang, P. Wang, Y. Tang, and W. Liu, "Analysis of dual band power and data telemetry for biomedical implants," *IEEE Trans. Biomed. Circuits Syst.*, vol. 6, no. 3, pp. 208–215, Jun. 2012.

[66] C.-Y. Wu, S.-H. Wang, and L.-Y. Tang, "CMOS high-efficiency wireless battery charging system with global power control through backward data telemetry for implantable medical devices," *IEEE Trans. Circuits Syst. I, Reg. Papers*, vol. 67, no. 12, pp. 5624–5635, Dec. 2020.

[67] Y. Park et al., "A wireless power and data transfer IC for neural prostheses using a single inductive link with frequency-splitting characteristic," *IEEE Trans. Biomed. Circuits Syst.*, vol. 15, no. 6, pp. 1306–1319, Dec. 2021.

[68] J. Pan, A. A. Abidi, W. Jiang, and D. Marković, "Simultaneous transmission of up to 94-mW self-regulated wireless power and up to 5-Mb/s reverse data over a single pair of coils," *IEEE J. Solid-State Circuits*, vol. 54, no. 4, pp. 1003–1016, Apr. 2019.

[69] R. Narayanamoorthi, "Modeling of capacitive resonant wireless power and data transfer to deep biomedical implants," *IEEE Trans. Compon., Packag. Manuf. Technol.*, vol. 9, no. 7, pp. 1253–1263, Jul. 2019.

[70] M. Kim, H.-S. Lee, J. Ahn, and H.-M. Lee, "A 13.56-MHz wireless power and data transfer system with current-modulated energy-reuse back telemetry and energy-adaptive voltage regulation," *IEEE J. Solid-State Circuits*, vol. 58, no. 2, pp. 400–410, Feb. 2023.

[71] Y. Zeng, C. Lu, R. Liu, X. He, C. Rong, and M. Liu, "Wireless power and data transfer system using multidirectional magnetic coupler for swarm AUVs," *IEEE Trans. Power Electron.*, vol. 38, no. 2, pp. 1440–1444, Feb. 2023.

[72] Z. Qian, R. Yan, J. Wu, and X. He, "Full-duplex high-speed simultaneous communication technology for wireless EV charging," *IEEE Trans. Power Electron.*, vol. 34, no. 10, pp. 9369–9373, Oct. 2019.

[73] C.-C. Huang, C.-L. Lin, and Y.-K. Wu, "Simultaneous wireless power/data transfer for electric vehicle charging," *IEEE Trans. Ind. Electron.*, vol. 64, no. 1, pp. 682–690, Jan. 2017.

[74] J.-J. Kao, C.-L. Lin, Y.-C. Liu, C.-C. Huang, and H.-S. Jian, "Adaptive bidirectional inductive power and data transmission system," *IEEE Trans. Power Electron.*, vol. 36, no. 7, pp. 7550–7563, Jul. 2021.

[75] H. Jung and B. Lee, "Wireless power and bidirectional data transfer system for IoT and mobile devices," *IEEE Trans. Ind. Electron.*, vol. 69, no. 11, pp. 11832–11836, Nov. 2022.

[76] H. Lee, K.-J. Lee, H. Kim, and I. Lee, "Wireless information and power exchange for energy-constrained device-to-device communications," *IEEE Internet Things J.*, vol. 5, no. 4, pp. 3175–3185, Aug. 2018.

[77] J.-G. Kim, G. Wei, M.-H. Kim, H.-S. Ryo, and C. Zhu, "A wireless power and information simultaneous transfer technology based on 2FSK modulation using the dual bands of series–parallel combined resonant circuit," *IEEE Trans. Power Electron.*, vol. 34, no. 3, pp. 2956–2965, Mar. 2019.

[78] H. Kennedy, R. Bodnar, T. Lee, and W. Redman-White, "28.4 a high-Q resonant inductive link transmit modulator/driver for enhanced power and FSK/PSK data transfer using adaptive-predictive phase-continuous switching fractional-capacitance tuning," in *Proc. IEEE Int. Solid- State Circuits Conf. (ISSCC)*, 2019, pp. 444–446.

[79] D. Ye, Y. Wang, Y. Xiang, L. Lyu, H. Min, and C.-J. R. Shi, "A wireless power and data transfer receiver achieving 75.4% effective power conversion efficiency and supporting 0.1% modulation depth for ASK demodulation," *IEEE J. Solid-State Circuits*, vol. 55, no. 5, pp. 1386–1400, May 2020.

[80] G. Elamary, G. Chester, and J. Neasham, "An analysis of wireless inductive coupling for high data rate biomedical telemetry using a new VHDL n-PSK modulator," in *Proc. 16th IEEE Int. Conf. Electron., Circuits Syst. (ICECS)*, 2009, pp. 211–214.

[81] Y. Sun, P.-X. Yan, Z.-H. Wang, and Y.-Y. Luan, "The parallel transmission of power and data with the shared channel for an inductive power transfer system," *IEEE Trans. Power Electron.*, vol. 31, no. 8, pp. 5495–5502, Aug. 2016.

[82] G. Wei, J. Feng, J. Zhang, C. Wang, C. Zhu, and S. Y. Ostanin, "An efficient power and data synchronous transfer method for wireless power transfer system using double-D coupling coil," *IEEE Trans. Ind. Electron.*, vol. 68, no. 11, pp. 10643–10653, Nov. 2021.

[83] J. Wu, C. Zhao, Z. Lin, J. Du, Y. Hu, and X. He, "Wireless power and data transfer via a common inductive link using frequency division multiplexing," *IEEE Trans. Ind. Electron.*, vol. 62, no. 12, pp. 7810–7820, Dec. 2015.

[84] J. Wu, S. Zong, and X. He, "Power/signal time division multiplexing technique based on power electronic circuits," in *Proc. 26th Annu. IEEE Appl. Power Electron. Conf. Expo. (APEC)*, 2011, pp. 1710–1714.

[85] F. Zhao, L. Wei, and H. Chen, "Optimal time allocation for wireless information and power transfer in wireless powered communication systems," *IEEE Trans. Veh. Technol.*, vol. 65, no. 3, pp. 1830–1835, Mar. 2016.

[86] X. Li, J. Hu, Y. Li, H. Wang, M. Liu, and P. Deng, "A decoupled power and data-parallel transmission method with four-quadrant misalignment tolerance for wireless power transfer systems," *IEEE Trans. Power Electron.*, vol. 34, no. 12, pp. 11531–11535, Jun. 2019.

[87] A. Liotta, E. Moisello, G. Frattini, P. Giannelli, P. Malcovati, and E. Bonizzoni, "A novel capacitive-inductive channel for wireless power and data transmission," in *Proc. ISCAS*, 2023, p. 1–5.

[88] H. Zheng, Z. Wang, Y. Li, and P. Deng, "Data transmission through energy coil of wireless power transfer system," in *Proc. IEEE PELS Workshop Emerg. Technol. Wireless Power Transf. (WoW)*, 2017, pp. 1–4.

[89] X. Li, C. Tang, X. Dai, P. Deng, and Y. Su, "An inductive and capacitive combined parallel transmission of power and data for wireless power transfer systems," *IEEE Trans. Power Electron.*, vol. 33, no. 6, pp. 4980–4991, Jun. 2018.

[90] Y. Zhang, T. Lu, Z. Zhao, F. He, K. Chen, and L. Yuan, "Selective wireless power transfer to multiple loads using receivers of different resonant frequencies," *IEEE Trans. Power Electron.*, vol. 30, no. 11, pp. 6001–6005, Nov. 2015.

[91] Y.-J. Kim, D. Ha, W. J. Chappell, and P. P. Irazoqui, "Selective wireless power transfer for smart power distribution in a miniature-sized multiple-receiver system," *IEEE Trans. Ind. Electron.*, vol. 63, no. 3, pp. 1853–1862, Mar. 2016.

[92] C. Luo, D. Qiu, W. Gu, B. Zhang, Y. Chen, and W. Xiao, "Multiload wireless power transfer system with constant output power and efficiency," *IEEE Trans. Ind. Appl.*, vol. 58, no. 1, pp. 1101–1114, Jan./Feb. 2022.

[93] R. Narayanamoorthi, A. V. Juliet, and B. Chokkalingam, "Cross interference minimization and simultaneous wireless power transfer to multiple frequency loads using frequency bifurcation approach," *IEEE Trans. Power Electron.*, vol. 34, no. 11, pp. 10898–10909, Feb. 2019.

[94] X. Xie, C. Xie, J. Wang, Y. Li, Y. Du, and L. Li, "Constant current output control based on cross-coupling compensation in multireceiver WPT system using active rectifier," *IEEE Trans. Transp. Electrific.*, vol. 9, no. 1, pp. 1960–1972, Mar. 2023.

[95] J. Song, M. Liu, and C. Ma, "Analysis and design of a high-efficiency 6.78-MHz wireless power transfer system with scalable number of receivers," *IEEE Trans. Ind. Electron.*, vol. 67, no. 10, pp. 8281–8291, Oct. 2020.

[96] B. Jang et al., "A 15-W triple-mode wireless power transmitting unit with high system efficiency using integrated power amplifier and DC–DC converter," *IEEE Trans. Ind. Electron.*, vol. 68, no. 10, pp. 9574–9585, Oct. 2021.

[97] P. S. Riehl et al., "Wireless power systems for mobile devices supporting inductive and resonant operating modes," *IEEE Trans. Microw. Theory Techn.*, vol. 63, no. 3, pp. 780–790, Feb. 2015.

[98] D. Ahn and P. P. Mercier, "Wireless power transfer with concurrent 200-kHz and 6.78-MHz operation in a single-transmitter device," *IEEE Trans. Power Electron.*, vol. 31, no. 7, pp. 5018–5029, Jul. 2016.

[99] J. T. Hwang et al., "21.8 an all-in-one (Qi, PMA and A4WP) 2.5W fully integrated wireless battery charger IC for wearable applications," in *Proc. IEEE Int. Solid-State Circuits Conf. (ISSCC)*, 2016, pp. 378–380.

[100] M. Huang, Y. Lu, U. Seng-Pan, and R. P. Martins, "22.4 a reconfigurable bidirectional wireless power transceiver with maximum-current charging mode and 58.6% battery-to-battery efficiency," in *Proc. IEEE Int. Solid-State Circuits Conf. (ISSCC)*, 2017, pp. 376–377.

[101] Y.-J. Park et al., "A triple-mode wireless power-receiving unit with 85.5% system efficiency for A4WP, WPC, and PMA applications," *IEEE Trans. Power Electron.*, vol. 33, no. 4, pp. 3141–3156, Apr. 2018.

[102] S.-J. Oh et al., "A 15-W quadruple-mode reconfigurable bidirectional wireless power transceiver with 95% system efficiency for wireless charging applications," *IEEE Trans. Power Electron.*, vol. 36, no. 4, pp. 3814–3827, Apr. 2021.

[103] J. H. Kim et al., "Development of 1-MW inductive power transfer system for a high-speed train," *IEEE Trans. Ind. Electron.*, vol. 62, no. 10, pp. 6242–6250, Mar. 2015.

[104] M. Kiani, B. Lee, P. Yeon, and M. Ghovanloo, "A Q-modulation technique for efficient inductive power transmission," *IEEE J. Solid-State Circuits*, vol. 50, no. 12, pp. 2839–2848, Jul. 2015.

[105] S. Samanta and A. K. Rathore, "A new current-fed CLC transmitter and LC receiver topology for inductive wireless power transfer application: Analysis, design, and experimental results," *IEEE Trans. Transp. Electrific.*, vol. 1, no. 4, pp. 357–368, Sep. 2015.

[106] C. Zhang, D. Lin, and S. Y. R. Hui, "Ball-joint wireless power transfer systems," *IEEE Trans. Power Electron.*, vol. 33, no. 1, pp. 65–72, Jan. 2018.

[107] F. Mao, Y. Lu, U. Seng-Pan, and R. P. Martins, "A reconfigurable cross-connected wireless-power transceiver for bidirectional device-to-device charging with 78.1% total efficiency," in *Proc. IEEE Int. Solid-State Circuits Conf. (ISSCC)*, 2018, pp. 140–142.

[108] M. Huang, Y. Lu, and R. P. Martins, "A reconfigurable bidirectional wireless power transceiver for battery-to-battery wireless charging," *IEEE Trans. Power Electron.*, vol. 34, no. 8, pp. 7745–7753, Aug. 2019.
[109] F. Mao, Y. Lu, and R. P. Martins, "A reconfigurable cross-connected wireless-power transceiver for bidirectional device-to-device wireless charging," *IEEE J. Solid-State Circuits*, vol. 54, no. 9, pp. 2579–2589, Jul. 2019.
[110] J. Pries, V. P. N. Galigekere, O. C. Onar, and G.-J. Su, "A 50-kW three-phase wireless power transfer system using bipolar windings and series resonant networks for rotating magnetic fields," *IEEE Trans. Power Electron.*, vol. 35, no. 5, pp. 4500–4517, May 2020.
[111] B. Luo, T. Long, L. Guo, R. Dai, R. Mai, and Z. He, "Analysis and design of inductive and capacitive hybrid wireless power transfer system for railway application," *IEEE Trans. Ind. Appl.*, vol. 56, no. 3, pp. 3034–3042, May 2020.
[112] H. Zhu, B. Zhang, and L. Wu, "Output power stabilization for wireless power transfer system employing primary-side-only control," *IEEE Access*, vol. 8, pp. 63735–63747, 2020.
[113] H. Oh et al., "Mid-range wireless power transfer system for various types of multiple receivers using power customized resonator," *IEEE Access*, vol. 9, pp. 45230–45241, 2021.
[114] Z. Yan et al., "Free-rotation wireless power transfer system based on composite anti-misalignment method for AUVs," *IEEE Trans. Power Electron.*, vol. 38, no. 4, pp. 4262–4266, Apr. 2023.
[115] H. Kim, Y. Park, and C. Kim, "A 13.56-MHz wireless power transfer system with a wide operating distance and load range for biometric smartcards," *IEEE Trans. Power Electron.*, vol. 38, no. 4, pp. 5576–5585, Apr. 2023.
[116] S.-U. Shin, M. Choi, S. Jung, H.-M. Lee, and G.-H. Cho, "A time-interleaved resonant voltage mode wireless power receiver with delay-based tracking loops for implantable medical devices," *IEEE J. Solid-State Circuits*, vol. 55, no. 5, pp. 1374–1385, May 2020.
[117] S.-H. Yang, K.-H. Chen, Y.-H. Lin, S.-R. Lin, and T.-Y. Tsai, "A temperature compensated 61-W class-E soft-switching GaN-based active diode rectifier for wireless power transfer applications," *IEEE Solid-State Circuits Lett.*, vol. 2, no. 9, pp. 203–206, Sep. 2019.
[118] G. Namgoong et al., "3–12-V wide input range adaptive delay compensated active rectifier for 6.78-MHz loosely coupled wireless power transfer system," *IEEE Trans. Circuits Syst. I, Reg. Papers*, vol. 68, no. 6, pp. 2702–2713, Jun. 2021.
[119] D. C. Corrêa, U. C. Resende, and F. S. Bicalho, "Experiments with a compact wireless power transfer system using strongly coupled magnetic resonance and metamaterials," *IEEE Trans. Magn.*, vol. 55, no. 8, pp. 1–4, May 2019.
[120] W. Lee and Y.-K. Yoon, "Tunable metamaterial slab for efficiency improvement in misaligned wireless power transfer," *IEEE Microw. Wireless Compon. Lett.*, vol. 30, no. 9, pp. 912–915, Aug. 2020.
[121] Z. Zheng, X. Fang, Y. Zheng, and H. Feng, "A wireless power transfer system based on dual-band metamaterials," *IEEE Microw. Wireless Compon. Lett.*, vol. 32, no. 6, pp. 615–618, Jun. 2022.

**ELISABETTA MOISELLO** (Member, IEEE) was born in Pavia, Italy, in 1993. She received the master's degree (summa cum laude) in electronic engineering and the Ph.D. degree in microelectronics from the University of Pavia, Pavia, Italy, in 2017 and 2020, respectively.

She is currently a Postdoctoral Research Fellow and a Contract Professor with the University of Pavia. Her research topics include sensory interface circuits, temperature-to-digital converters, switching dc–dc converters, and wireless power transfer.

**ALESSANDRO LIOTTA** (Graduate Student Member, IEEE) was born in Catania, Italy, in 1997. He received the bachelor's degree in electronic engineering from the University of Catania, Catania, Italy, in 2019, and the master's degree (summa cum laude) in electronic engineering from the University of Pavia, Pavia, Italy, in 2021, where he is currently pursuing the Ph.D. degree in microelectronics.

His current research topic is the design of simultaneous wireless information and power transfer systems.

**PIERO MALCOVATI** (Senior Member, IEEE) received the Laurea degree in electronic engineering from the University of Pavia, Pavia, Italy, in 1991, and the Ph.D. degree in electrical engineering from ETH Zürich, Zürich, Switzerland, in 1996.

From 1996 to 2001, he was an Assistant Professor and from 2002 to 2017, an Associate Professor with the Department of Electrical, Computer, and Biomedical Engineering, University of Pavia, where he has been a Full Professor since 2017. His research activities are focused on microsensor interface circuits, power electronics circuits, and high-performance data converters.

Prof. Malcovati was and still is a member of the Technical Program Committees for several International Conferences, including ISSCC, ESSCIRC, SENSORS, ICECS, and PRIME. He is an Associate Editor of the IEEE JOURNAL OF SOLID-STATE CIRCUITS.

**EDOARDO BONIZZONI** (Senior Member, IEEE) received the Laurea degree (summa cum laude) in electronic engineering and the Ph.D. degree in electronic, computer, and electrical engineering from the University of Pavia, Pavia, Italy, in 2002 and 2006, respectively.

He is currently an Associate Professor with the Department of Electrical, Computer, and Biomedical Engineering, University of Pavia. His current research interests are focused on the design and testing of A/D converters, dc–dc converters, high-precision amplifiers, and sensor interfaces.

Dr. Bonizzoni has been an Associate Editor of the IEEE TRANSACTIONS ON CIRCUITS AND SYSTEMS I: REGULAR PAPERS from 2016 to 2019. He is currently an incoming Editor-in-Chief of the IEEE TRANSACTIONS ON CIRCUITS AND SYSTEMS II: EXPRESS BRIEFS for the 2024–2025 term and a TPC Member of IEEE CICC.

Open Access funding provided by 'Università degli Studi di Pavia' within the CRUI CARE Agreement